Frequency tunable gyrotron using backward-wave components

JOURNAL OF APPLIED PHYSICS 105, 063304 (2009)

Frequency tunable gyrotron using backward-wave components

T. H. Chang,[1,2,a] T. Idehara,[2] I. Ogawa,[2] L. Agusu,[2] and S. Kobayashi[2]
[1]*Department of Physics, National Tsing Hua University, Hsinchu, 300, Taiwan*
[2]*Research Center for Development of Far-Infrared Region, Fukui University (FIR FU), Fukui 910-8507, Japan*

(Received 4 November 2008; accepted 6 February 2009; published online 24 March 2009)

We report a frequency tunable scheme for the gyrotron at millimeter/submillimeter regime. Unlike the step-tunable type where oscillation frequencies change discretely, this scheme continuously adjusts the oscillation frequency as the magnetic field varies. It is a hybrid system, taking the advantages of the backward-wave interaction and the converter-free output structure. The characteristics of backward-wave interaction will be shown. A proof of principle experiment was conducted with a scaled cavity. The result shows the oscillation frequency smoothly transitions over a wide range of 6 GHz from 134 to 140 GHz. With proper design this mechanism is capable of producing medium output power with broad frequency tunability up to the terahertz region. © *2009 American Institute of Physics*. [DOI: 10.1063/1.3097334]

I. INTRODUCTION

The gyrotron oscillators, capable of producing high power in millimeter and submillimeter wave regions, have widespread applications,[1] for example, heating of the fusion plasmas,[2,3] measurement of the electron spin resonance (ESR),[4,5] and the sensitivity enhancement of nuclear magnetic resonance using the dynamic nuclear polarization technique (DNP NMR).[6–8] The DNP NMR experiment requires a stable continuous-wave (cw) power of several tens of watts at a very high frequency, e.g., 460 GHz.[8] Second cyclotron harmonic interaction is preferred. However, the interaction strength of the second harmonic is weak. A long interaction structure with high quality factor is generally required. Therefore the oscillation frequency range is limited and is difficult to meet the DNP NMR experimental requirement. There is a pressing need for gyrotron with frequency tunability.

Gyrotrons with stepwise frequency tunability have been developed for years.[9] The oscillation frequency jumps from one transverse mode to another as the magnetic field is adjusted. Its frequency is basically proportional to the cyclotron frequency or its harmonics, but not continuously tunable. On the other hand, the gyrotron backward-wave oscillator (gyro-BWO) is formed by the internal feedback at a nonresonant structure. The oscillation frequency is tunable, but, to extract the wave power, a high performance mode converter must be built, which is extremely difficult at the terahertz range. In the early phase of gyro-BWO development, however, mode converters are generally unavailable. The generated wave power propagates backward, hits the end reflection, and then comes out at the downstream. This type of oscillator is called the reflected gyro-BWO.[10,11] Its operation frequency is normally close to the waveguide cutoff.

This study employs a configuration similar to the reflected-type gyro-BWO but puts emphasis on the frequency tunability. Unlike step-tunable gyrotron where oscillation jumps discretely in different transverse modes, this approach allows a smooth tuning within a single transverse mode using its backward-wave components. The characteristics of backward-wave interaction will be shown. A proof of principle experiment was conducted using the Gyrotron FU CW IV in Far-Infrared Region, Fukui University (FIR FU). Results verified that this frequency tunable scheme is capable of achieving continuous frequency tuning over a wide range.

II. CHARACTERISTICS OF BACKWARD-WAVE INTERACTION

The oscillator version of the gyrodevices by feedback mechanism can be classified into gyromonotron and gyro-BWO.[12,13] The former is formed by the reflective feedback, where its tunability is limited by the resonant condition of the interaction cavity.[9,11] So the oscillation frequency is basically fixed. The latter is formed by the internal feedback. The oscillation frequency can be adjusted by either changing the magnetic field or the beam voltage. However, extracting the wave energy at the upstream section is difficult, imposing a severe limitation to gyro-BWO, especially at the submillimeter wave regime.

We employ a hybrid gyrotron, i.e., the reflected gyro-BWO. The wave is extracted at the downstream (advantage of gyromonotron, no mode converter is needed), while the feedback mechanism is mainly internal (advantage of gyro-BWO, broad tuning range). The interaction structure is the cavity type with a reduced quality factor. Table I summarizes the simulation and experimental parameters.

Figure 1(a) shows the calculated starting currents for two structures, the uniform structure and the mildly tapered structure as shown in the inset. In the simulation, the radius of the main interaction section is 0.2372 cm. The length of the upstream taper is 0.4 cm long, while the output section is a linear taper of 3.0°. The dashed line is obtained with a uniform section of 2.5 cm. To demonstrate the effect of end reflection, the solid line is calculated using a 2.0 cm uniform

[a]Electronic mail: thschang@phys.nthu.edu.tw.

TABLE I. Parameters for simulation and proof of principle experiment.

Parameter	Simulation	Experiment
Operating mode	$TE_{0,6,1}$	$TE_{1,2,1}$
Cyclotron harmonic	Second	Fundamental
L_0 (cm)	2.0+0.5	2.0
r_w (cm)	0.2732	0.190
Cutoff frequency (at r_w) (GHz)	394.581	133.97
Beam current (I_b) (A)	0.35	0.4
Beam voltage (V_b) (kV)	13.7	19.0
Magnetic field (B_0) (T)	7.2–7.45	4.75–5.3
Frequency tuning range (GHz)	394–399	134–140
Guiding center position (r_c)	$0.16r_w$	$0.2r_w$
Velocity ratio ($\alpha=v_\perp/v_z$)	1.6	1.0
Velocity spread ($\Delta v_z/v_z$) (%)	0%	0%

section plus a 0.5 cm mild taper of 0.12°. The broader resonant width of high-order axial modes (HOAMs) results in a greater mode overlapping. This self-consistent effect on the starting current has early been found before,[15] but it attracts attention until recently.[7,16]

It is worth to note here that the starting current for the uniform structure (dashed line) varies dramatically when the magnetic field changes. The ratio between the operating current (350 mA) and the lowest starting current (22 mA) is 16, which is too high and will cause nonstationary behavior.[17–19] On the other hand, a slightly modified structure (solid line) effectively evens the starting current. Detailed studies regarding the effect of the end reflection can be found in Refs.

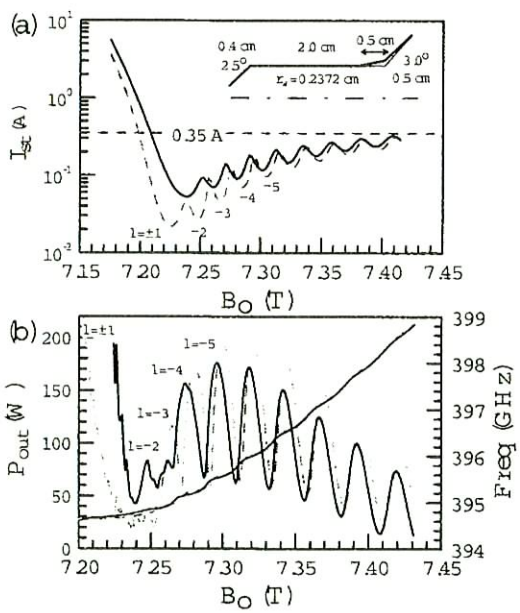

FIG. 1. (Color online) (a) The starting currents vs the magnetic field obtained with a self-consistent code. (b) The output power and frequency vs the magnetic field at a beam current of 0.35 A. The inset shows two interaction structures, uniform and mildly tapered, not drawn to scale. The results of a uniform cavity are represented in dashed lines and those of a mildly tapered cavity are depicted in solid lines. All the parameters used are shown in Table I.

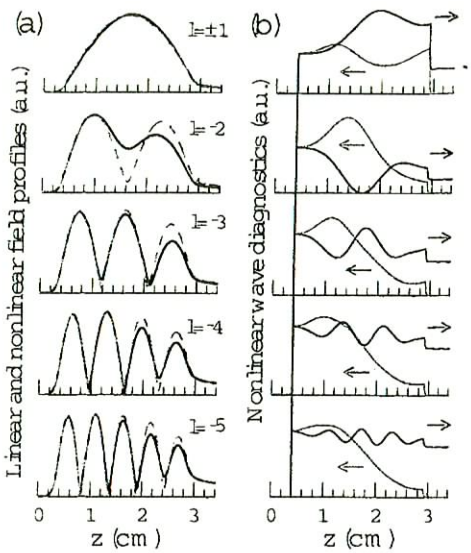

FIG. 2. (Color online) The wave diagnostics for uniform cavity. (a) The field profiles at linear (starting current) and nonlinear (0.35 A) stages. (b) The forward-wave and backward-wave energy is indicated with arrows.

20 and 21. The greatest starting current ratio is then reduced to 6.6, which happens to be marginally stable.

Figure 1(b) shows the output power and the oscillation frequency versus the magnetic field for the two structures mentioned in Fig. 1(a). The power of the fundamental mode is, as usual, the largest compared to other axial modes. The output power basically forms a fingerlike shape. Note that, in the mode transition region, the output power is nonzero and the oscillation frequency can be smoothly tuned. The envelope of the lowest output power is still higher than the need for DNP NMR application (a few tens of watts, see Ref. 8).

The mildly tapered structure (solid line) is superior to the uniform structure (dashed line) in that the neck of the output power (around $l=-2$) is higher. The mild taper reduces the structure reflection and allows the backward-wave interaction to be dominant. In addition, the mild taper reduces the quality factor, resulting in stronger mode overlapping, which smoothes power spectrum. The velocity spread plays a minor role when the oscillation is close to the waveguide cutoff. Thus, zero spread is used. The crests and troughs in the power spectrum can be further smoothed provided better matching circuit is used.

Figure 2(a) shows the calculated linear and nonlinear field profiles of the first five axial modes. The profiles are normalized to unity. The field diagnosis is basically consistent with the results found in Ref. 7. More characteristics of the backward-wave interaction are elaborated here. The linear field profiles (dashed lines) are taken at their perspective starting current, while the nonlinear (solid lines) are the results at 0.35 A. The linear field profiles are basically determined by the structure resonance. The profiles of the fundamental mode do not change, implying that the feedback mechanism remains reflective. HOAMs ($l=-2,-3,-4\ldots$), however, exhibit different behaviors. The last crest of the

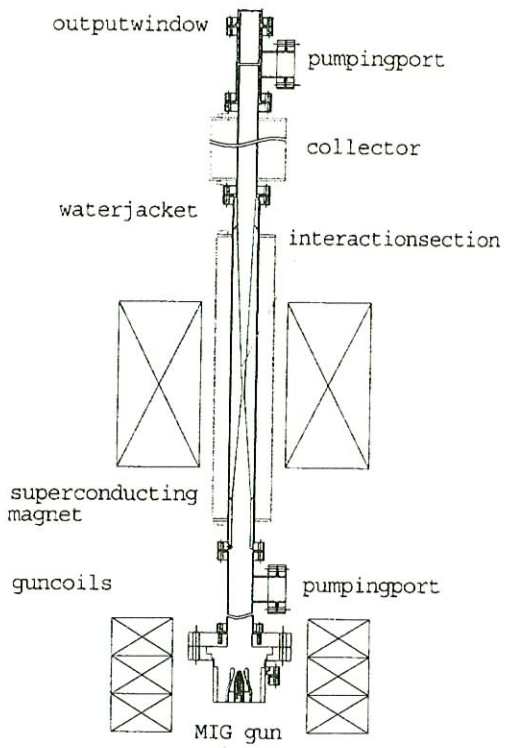

FIG. 3. (Color online) A schematic of the gyrotron system (named as Gyrotron FU CW IV). A demountable tube is installed on the axis of the magnetic system of a 10 T superconducting magnet and three additional coils.

field profile of each HOAM at nonlinear stage always lowers than that at linear stage. This is the evidence of the nonlinear field contraction. The effect is unique to gyro-BWO.[22]

Figure 2(b) displays the wave diagnostics at nonlinear stage for the first five axial modes. The wave is decomposed into forward wave and backward wave, indicated with arrows. The fundamental mode ($l=\pm 1$) exhibits a reflective feedback. The sudden drop of the forward wave energy at the interface of the uniform section and taper section is caused by the reflection effect. The reflected (backward) wave interacts with the beam and then bounces back at the upstream cutoff section. However, the HOAMs ($l=-2,-3,-4,-5$) exhibit a different behavior. The reflection is generally reduced. The reflective feedback becomes less important, while the internal feedback plays a dominant role. The backward wave energy is peaking at the beam entrance. This is a strong evidence of the backward-wave interaction. Since the beam is selectively interacting with the backward-wave component of an axial mode, the mode index is thus shown in the negative value. Note that as the beam current rises much higher than the starting current, the operating axial mode of a low-Q cavity might transition to another axial mode in order to meet the optimal resonant condition.[17]

III. EXPERIMENTAL RESULTS

To prove the principle, an existing gyrotron system (Gyrotron FU cw IV) was used. It is a scaled experiment. The

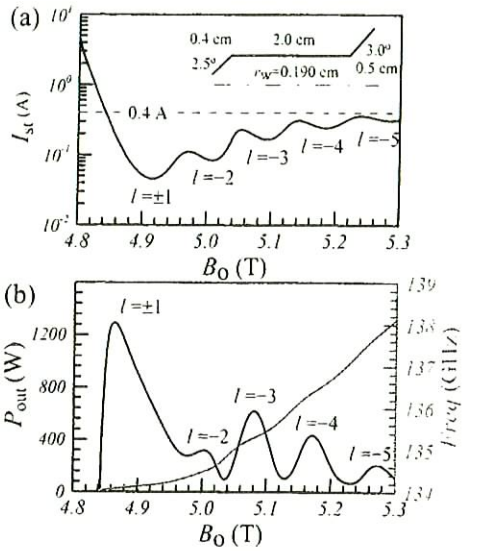

FIG. 4. (Color online) The linear and nonlinear characteristics for the TE_{12} mode. (a) The starting currents vs the magnetic field. (b) The output power and frequency vs the magnetic field at a beam current of 0.4 A. The inset shows the actual interaction structure. All the parameters used are shown in Table I.

experimental parameters are shown in Table I. It is operated at the TE_{12} mode with fundamental cyclotron harmonic. A schematic of the system is shown in Fig. 3. The electron beam is generated by a triode magnetron injection gun with adjustable anode voltage and cathode voltage. In practice, the electron beam parameters such as the beam radius and velocity pitch factor can be adjusted by the gun coils. The axis of the interaction structure is aligned with that of 10 T superconducting magnetic. For the cw operation, the ambient temperature is controlled with a water cooling system. The tube is maintained at 27 °C. The interaction structure is scaled for the TE_{12} mode. The radius (r_w) and the length (L_0) of the cavity are 0.190 and 2.0 cm, respectively. The upstream cutoff is a taper section of 2.5° and the downstream section is a linear taper of 3°, all the way to the collector of the inner radius of 2.8 cm. The spent electron beam is dumped onto the collector. The collector also serves as a waveguide, guiding the wave to the output window. The output spectrum is detected with a pyroelectric detector and recorded with an XY recorder. The output power is measured with a water load and the frequency is detected with a down converting mixer and a spectrum analyzer.

Figure 4 shows the simulated results using the single mode particle tracing code. The TE_{12} mode is expected to be oscillated at the experimental condition. The starting-current curve is plotted in Fig. 4(a) and the interaction structure is inset at the upper-right corner. The nonlinear behavior at the beam current of 0.4 A is displayed in Fig. 4(b). In comparison with Fig. 1, the number of the axial modes is reduced due to a shorter effective-interaction length ($L_{eff}=L_0/\lambda_g$, where λ_g is the guide wavelength). The L_{eff} for TE_{06} and TE_{12} modes are 2.6 and 1.2, respectively. The finger-shape

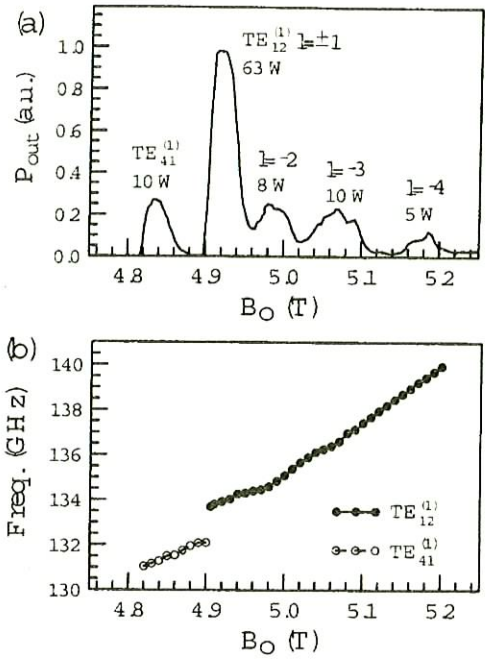

FIG. 5. The measured results of a scaled proof-of-principle experiment. (a) The output power spectrum and (b) the oscillation frequency vs the magnetic field. The experimental parameters are shown in Table I.

tuning curve shown in Fig. 1(b) is verified again in Fig. 4(b). These two figures illustrate the similar trend that the backward-wave component of the axial modes could smoothly tune in frequency.

Figure 5 shows the measured results. The output spectrum is plotted in Fig. 5(a) and the oscillation frequency is depicted in Fig. 5(b). In this scaled experiment, two transverse modes are found, TE_{41} and TE_{12}. These two transverse modes are all operated at the fundamental cyclotron harmonic. Each operates at different magnetic field. The transverse-mode competition is less severe. The output power spectrum shows the finger shape as predicted. The output power of each peak is marked on the figure. The measured nonlinear behavior [Figs. 5(a) and 5(b)] agrees qualitatively with the theoretical prediction [Fig. 4(b)], but the measured power is much lower than the calculated value and the measured frequency is slightly higher than the calculated result. The reasons might be attributed to the beam parameters used in simulation. The beam parameters, like the pitch factor, the guiding center, and the velocity spread, can be adjusted with the triode electron gun. In addition, the pitch factor and the velocity spread are functions of the magnetic field. Note that although the efficiency is low, the frequency is tunable over a broad range of 6 GHz from 134 to 140 GHz.

IV. CONCLUSION

In summary, we demonstrated that a frequency tunable scheme for the gyrotron is feasible. The electron beam interacts with the backward-wave component. They form an internal feedback loop and allow the oscillation to be smoothly tuned over a broad range. A proof of principle experiment was conducted using a set of scaled parameters and demonstrated a very broad frequency tuning range of 6 GHz (~4.5%). This implies a tradeoff between the bandwidth and efficiency which can be exercised in accordance with the specific application need. There is room for efficiency improvement. A detailed research is underway to design a less reflective circuit and to develop a transverse mode selective circuit in the hope of achieving a much higher efficiency and a much broader bandwidth at terahertz region.

ACKNOWLEDGMENTS

This work was sponsored by the National Science Council of Taiwan and Japanese Society for Promotion of Science. The authors are grateful to Professor K. R. Chu for many helpful discussions and Dr. C. C. Chiu for the technical support.

[1]M. Thumm, Int. J. Infrared Millim. Waves **22**, 377 (2001).
[2]H. Bindslev, S. K. Nielsen, L. Porte, J. A. Hoekzema, S. B. Korsholm, F. Meo, P. K. Michelsen, S. Michelsen, J. W. Oosterbeek, E. L. Tsakadze, E. Westerhof, P. Woskov, and the TEXTOR team, Phys. Rev. Lett. **97**, 205005 (2006).
[3]K. Sakamoto, A. Kasugai, K. Takahashi, R. Minami, N. Kobayashi, and K. Kajiwara, Nat. Phys. **3**, 411 (2007).
[4]S. Aripin, T. Mitsudo, K. Shirai, T. Matsuda, T. Kanemaki, T. Idehara, and T. Tatsukawa, Int. J. Infrared Millim. Waves **20**, 1875 (1999).
[5]S. Mitsudo, T. Aripin, T. Shirai, T. Matsuda, T. Kanemaki, and T. Idehara, Int. J. Infrared Millim. Waves **21**, 661 (2000).
[6]L. R. Becerra, G. J. Gerfen, R. J. Temkin, D. J. Singel, and R. G. Griffin, Phys. Rev. Lett. **71**, 3561 (1993).
[7]M. K. Hornstein, V. S. Bajaj, R. G. Griffin, K. E. Kreischer, I. Mastovsky, M. A. Shapiro, J. P. Sirigiri, and R. J. Temkin, IEEE Trans. Electron Devices **52**, 798 (2005).
[8]T. Idehara, I. Ogawa, L. Agusu, T. Kanemaki, S. Mitsudo, T. Saito, T. Fujiwara, and H. Takahashi, Int. J. Infrared Millim. Waves **28**, 433 (2007).
[9]T. Idehara, I. Ogawa, S. Mitsudo, M. Pereyaslavets, N. Nishida, and K. Yoshida, IEEE Trans. Plasma Sci. **27**, 340 (1999).
[10]R. H. Pantell, Proc. IRE **47**, 1146 (1959).
[11]S. Y. Park, N. Vanderplaats, S. Ahn, A. K. Ganguly, R. K. Parker, and V. L. Granatstein, IEEE Trans. Plasma Sci. **13**, 404 (1985).
[12]G. S. Nusinovich, *Introduction to the Physics of Gyrotrons* (John Hopkins University Press, Maryland, 2004).
[13]K. R. Chu, Rev. Mod. Phys. **76**, 489 (2004).
[14]L. Agusu, T. Idehara, I. Ogawa, T. Saito, T. Kanemaki, H. Takahashi, and T. Fujiwara, Int. J. Infrared Millim. Waves **28**, 499 (2007).
[15]V. L. Bratman and M. A. Moiseev, Radiophys. Quantum Electron. **18**, 722 (1975).
[16]T. H. Chang, K. F. Pao, S. H. Chen, and K. R. Chu, Int. J. Infrared Millim. Waves **24**, 1415 (2003).
[17]N. S. Ginzburg, G. S. Nusinovich, and N. A. Zavolsky, Int. J. Electron. **61**, 881 (1986).
[18]G. S. Nusinovich, A. N. Vlasov, and T. M. Antonsen, Jr., Phys. Rev. Lett. **87**, 218301 (2001).
[19]T. H. Chang, S. H. Chen, L. R. Barnett, and K. R. Chu, Phys. Rev. Lett. **87**, 064802 (2001).
[20]O. Dumbrajs, M. Thumm, J. Pretterebner, and D. Wagner, Int. J. Infrared Millim. Waves **13**, 825 (1992).
[21]E. Borie, Int. J. Infrared Millim. Waves **29**, 113 (2008).
[22]S. H. Chen, K. R. Chu, and T. H. Chang, Phys. Rev. Lett. **85**, 2633 (2000).